

Intrinsic Half-metallicity in Edge Fluorinated Armchair Boron Nitride Nanoribbons

Hari Mohan Rai¹ ‡, Shailendra K Saxena¹, Vikash Mishra¹, Ravikiran Late¹, Rajesh Kumar¹, Pankaj R Sagdeo¹, Neeraj K. Jaiswal² and Pankaj Srivastava³

¹ Material Research Laboratory, Discipline of Physics & MSEG, School of Basic Sciences, Indian Institute of Technology Indore, Madhya Pradesh-452017, India

² Discipline of Physics, PDPM- Indian Institute of Information Technology, Design and Manufacturing, Jabalpur 482005, India

³ Computational Nanoscience and Technology Lab. (CNTL), ABV- Indian Institute of Information Technology and Management, Gwalior 474015, India

Abstract. We predict intrinsic half-metallicity in armchair boron nitride nanoribbons (ABNNRs) via edge fluorination. The stability, electronic and magnetic properties of bare and edge fluorinated ABNNRs have been systematically analyzed by means of first-principles calculations within the local spin-density approximation (LSDA). The ribbons whose only edge-B atoms passivated with F atoms (i.e., edge-N atoms are unpassivated), regardless of width, are found half-metallic with a half-metal gap of 0.3 eV. A 100 % spin polarized charge transport across the Fermi level is expected for such ribbons as the spin polarized states are ~ 0.4 eV more stable than the spin un-polarized states and only single-spin conducting channels are present across the Fermi level owing to the gigantic spin splitting. The existence of half-metallicity is attributed to the localization of electronic charge at bare edge-N atoms as revealed from the analysis of Bloch states and projected density of states (PDOS). The sufficiently large half-metal gap (0.3 eV) with huge difference in the energies (~ 0.4 eV) of spin polarized and spin compensated states projects these half-metallic ABNNRs as potential candidate for spintronics applications.

1. Introduction

The discovery of single atom thick sheet of hexagonal boron nitride (h-BN) has invigorated theoretical as well as experimental research activities associated with h-BN nanomaterials. [1-4] This quasi-two-dimensional (2D) h-BN sheet has large energy band gap ($\sim 5\text{eV}$) which ensures its stability at elevated temperatures and thus makes it a promising candidate for high temperature semiconductor devices. Quasi-1-D thin strips carved out of h-BN sheet also exhibit excellent structural stability and distinct electronic properties as compared to parent h-BN sheet due to the quantum confinement effects. [4] These strips are formally known as boron nitride nanoribbons (BNNRs). Chen. et al. [5] have already synthesized hollow BNNRs through evaporation using BNOFe as precursor and ZnS nanoribbons as templates. Similar to their organic counterparts - Graphene Nanoribbons (GNRs), BNNRs can also be fabricated from a single h-BN layer via lithographic patterning. [6] According to the definite shape of edges BNNRs are mainly of two type i.e. zigzag boron nitride nanoribbons (ZBNNRs) and armchair boron nitride nanoribbons (ABNNRs). BNNRs exhibit fascinating and outstanding electronic properties similar to that of GNRs, [7,8] which are very important for the application in advanced devices. The electronic band gap (E_g) of ABNNRs passivated by H, oscillates periodically as a function of their width [9] whereas the band gap of ZBNNRs decreases monotonically when both the edges are H-passivated. [10,11] Owing to high efficiency and low power consumption, spintronic devices are attracting considerable attention nowadays. Being the key property for spin transport based electronics, Half-metallicity, has been vastly predicted and studied in different nanostructures [12-14] along with many other compounds like alloys (including ternary and quaternary Heusler alloys), [15-17] double layer perovskites, [18,19] transition metal pnictides, and chalcogenides in zinc blende phase. [20-22] Recently, the existence of a large spin polarization of (93_{-11}^{+8}) % has been directly evidenced at room temperature in an epitaxial thin film of Co_2MnSi . [23] First principle calculations have shown that half-metallicity may be realized also in BNNRs either by chemically functionalizing zigzag edges with different groups such as H and F or with the application of an external in-plane electric field. [24-26] In previous study on ZBNNRs [10], it is predicted that one-edge (only B-edge) H-passivation makes the ribbons ‘semi-metallic’ unlike the ‘half-metallic’ as predicted by Zheng et al. [24], but for spin polarized transport, both of these results are consistent with each other. Moreover, half-metallicity has also been perceived theoretically in ZBNNRs via percentage hydrogenation, [27] hybridization (through carbon in BC_2N nanoribbons), [28] and also through structural modifications (e.g., by making stirrup, boat, twist-boat etc.). [29] Conversely, in case of ABNNRs, half-metallicity has been predicted in hybrid armchair BCN- nanoribbons. [30] However, ABNNRs are almost unexplored towards the existence of spin polarization/half-metallicity. Therefore, in the present article, we have investigated the possibility of half-metallicity or spin polarization in ABNNRs via edge fluorination. Here, we predict manifestation of intrinsic half-metallicity in ABNNRs when only edge-B atoms are passivated with F atoms. In

addition, this article presents detailed and systematic analysis of structural stability, electronic and magnetic properties for bare and edge fluorinated ABNNRs with different widths. Present analysis shows that edge fluorination transforms bare ABNNRs into ferromagnetic/antiferromagnetic half-metals as energetically most favorable structures unlike hydrogenated nonmagnetic semiconductor as predicted by Ding et al. [31]

2. Computational details

The first-principles calculations were performed with Atomistix Tool Kit-Virtual NanoLab (ATK-VNL) [32] under the framework of density functional theory (DFT). The exchange correlation energy was approximated by local spin density approximation (LSDA) as proposed by Perdew and Zunger. [33] The reason for selecting LDA is that the generalized gradient approximation underestimates the surface impurity interactions. [34] The ABNNRs were modeled with periodic boundary conditions along z-axis, whereas the other two dimensions were confined. The energy cutoff value of 100 Rydberg was selected for the expansion of plane waves. We implemented double ζ plus polarized basis set for all the calculations. The k-point sampling was selected to $1 \times 1 \times 100$. In order to avoid artificial inter-ribbon interactions, ribbons were separated using a cell padding vacuum region of 10 Å. All the atoms were relaxed and, optimization of the atomic structures including atomic positions has been carried out until the forces on each individual atom were reduced to less than a 0.05 eV/. We represent the ribbon-width by a width parameter N_a , defined as the number of B/N atoms along the ribbon width as depicted in Figure 1, therefore, ABNNR with n B/N atoms is named as n-ABNNR.

3. Results and Discussion

In the present study, we have considered three different ABNNR structures (i) no passivation (bare ABNNR), (ii) both the edges fully passivated with F atoms (ABNNR_{FBN}) and (iii) both the edges partially/half passivated with F atoms. Furthermore, the ABNNRs belonging to third category are divided into two subgroups i.e., ABNNR_{FB} and ABNNR_{FN} depending upon whether only B or only N edge atoms are passivated by F atoms respectively. All these categories are depicted schematically in Figure 1. In order to take size effects into consideration, we investigate ABNNRs having widths $N_a = 6$ to 10. Since the findings are qualitatively similar, we displayed the figures only for ABNNRs with $N_a = 9$. Figure 1 schematically represents optimized geometry of ABNNR in all four considered ribbon configurations with $N_a = 9$ as representative case. The convention of super cell, we used for simulation is depicted by solid rectangles. First of all, in order to examine the relative stability of considered ribbon configurations, cohesive energy (E_c) has been calculated by using the following formula:

$$E_c = \frac{1}{(x + y + z)} \left[E_{tot}^{ABNNR} - (xE_{atom}^B + yE_{atom}^N + zE_{atom}^F) \right] \quad (1)$$

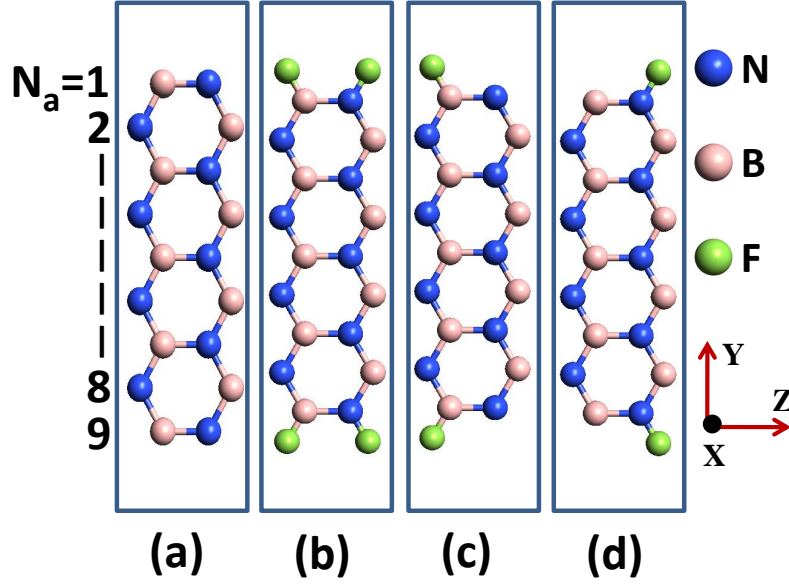


Figure 1. Convention of ribbon width and the supercell units ($N_a=9$) for (a) bare ABNNR, (b) ABNNR_{FBN}, (c) ABNNR_{FB} and (d) ABNNR_{FN}. The ABNNRs are modeled with periodic boundary conditions along z-axis whereas x and y directions are confined.

where E_{tot}^{ABNNR} , $x E_{atom}^B$, $y E_{atom}^N$ and $z E_{atom}^F$ are the total energies of ABNNR, free B atom, N atom and F atom, respectively; x, y and z are the number of B, N and F atoms in the super cell. The cohesive energies calculated for considered ribbon structures are summarized in Table 1. It is clear from Table 1 that bare ribbons are energetically most favorable. Further, the wider ribbons are relatively more stable. Since electronic and magnetic properties of the BNNRs depend critically on the type of edge passivation (partial/full), the knowledge of stability as a function of edge fluorination is of worth importance. The perusal of Table 1 indicates that irrespective of their width ABNNR_{FB} structures are energetically most stable out of all three edge fluorinated configurations as the minimum difference in E_c is 330 meV for 10-ABNNR_{FB} and 10-ABNNR_{FN}. This difference is large enough for any room temperature functioning. Present stability analysis predicts that amongst fluorinated ABNNRs, the probability of experimental realization is highest for ABNNR_{FB} structures. Being energetically the most stable ribbon structures, the results for all ABNNR_{FB} structures are addressed with greater detail in the next section. The calculated electronic band structure and density of states (DOS) for 9-ABNNR_{FB} are illustrated in Figures 2 (a) and (b) respectively. A substantial difference in the form of giant splitting of spin states can be clearly observed in both band structure as well as DOS profile. The spindown channels/states [Figures 2 (a)] are metallic with red bands almost crossing/touching the Fermi level (green dotted line) whereas owing to the manifestation of a large band gap of 4.75 eV the spin-up (black) states are insulating. Thus, we predict that the charge transport across the Fermi level through all ABNNR_{FB} structures is completely subjugated by the spin-

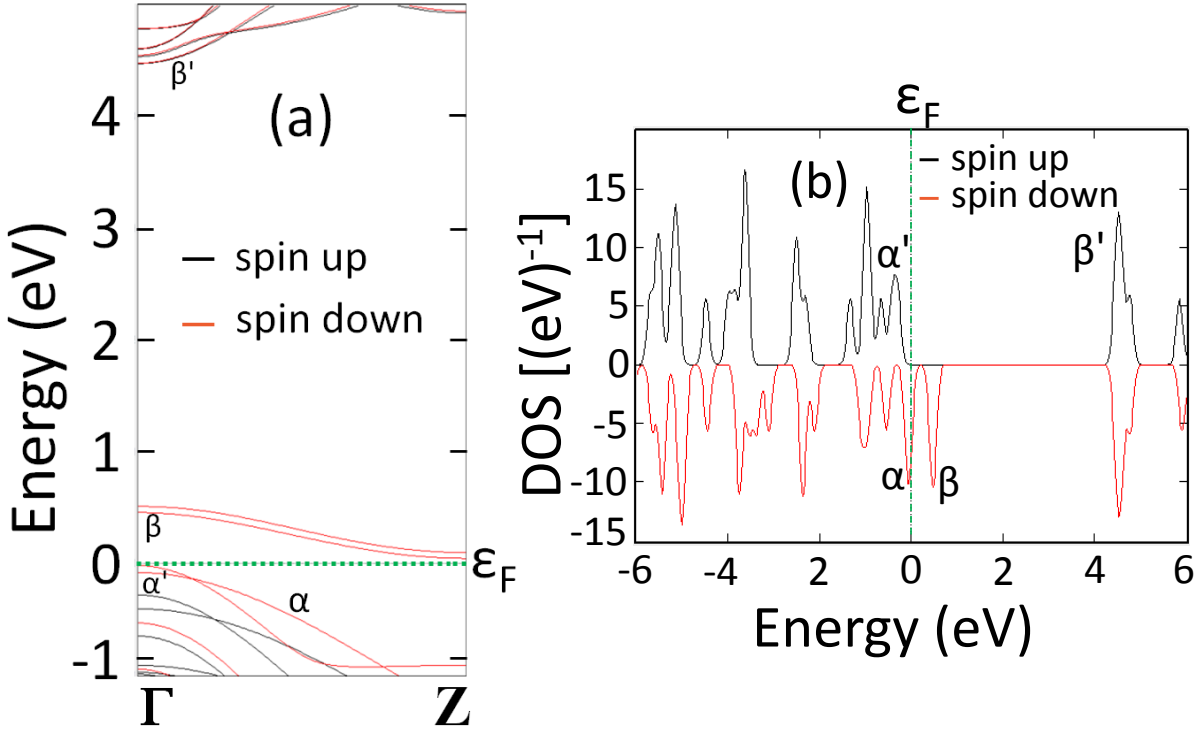


Figure 2. Calculated (a) electronic band structure and (b) density of states (DOS) for 9-ABNNR_{FB}. The spindown (spin-up) states nearest to the Fermi level in valence band and conduction band are indexed with α (α') and β (β') respectively. The Fermi level is indicated by green dotted line whereas spindown (spin-up) states are shown with red (black) color.

down electrons as also confirmed via DOS profile [Figures 2 (b)] in the form of crossing of Fermi level by a peak corresponding to spindown states. Thus it is expected that the current flow through such systems should be entirely spin polarized. The half-metal gap (i.e., the gap between topmost occupied spin-up band and Fermi level) of 0.3 eV has been witnessed which is very high as compared to the room temperature thermal energy (26 meV) and also comparable to the earlier reported values for half-metallic ZBNNRs and GNRs. [24,35] Figure 3 [(a)(c)] displays the electronic band structures and corresponding DOS for remaining three configurations ($N_a=9$, as a representative). It is obvious from figures 3 [(a) and (b)] that bare ABNNRs and ABNNR_{FBN} are insulating ($E_g > 4.2$ eV) in nature with degenerate spindown and spin-up bands. The DOS also reflect this wide band gap behavior as a separation between the peaks of corresponding spins across Fermi level whereas mirror symmetry appeared in the peaks of opposite spin-states reflects the spin degeneracy. In contrary, ABNNR_{FN} shows

breaking of spin degeneracy (mirror symmetry) as depicted in equivalent band structure (DOS profile) with a wide semiconducting band gap as can be seen in Figure 3 (c). Moreover, the width dependence of band gap is illustrated in the inset of Figure 3 (a) and (b) respectively. An oscillating behavior is observed for bare ABNNRs and $ABNNR_{FBN}$ which is a characteristic signature of ABNNRs. [9] In order to understand

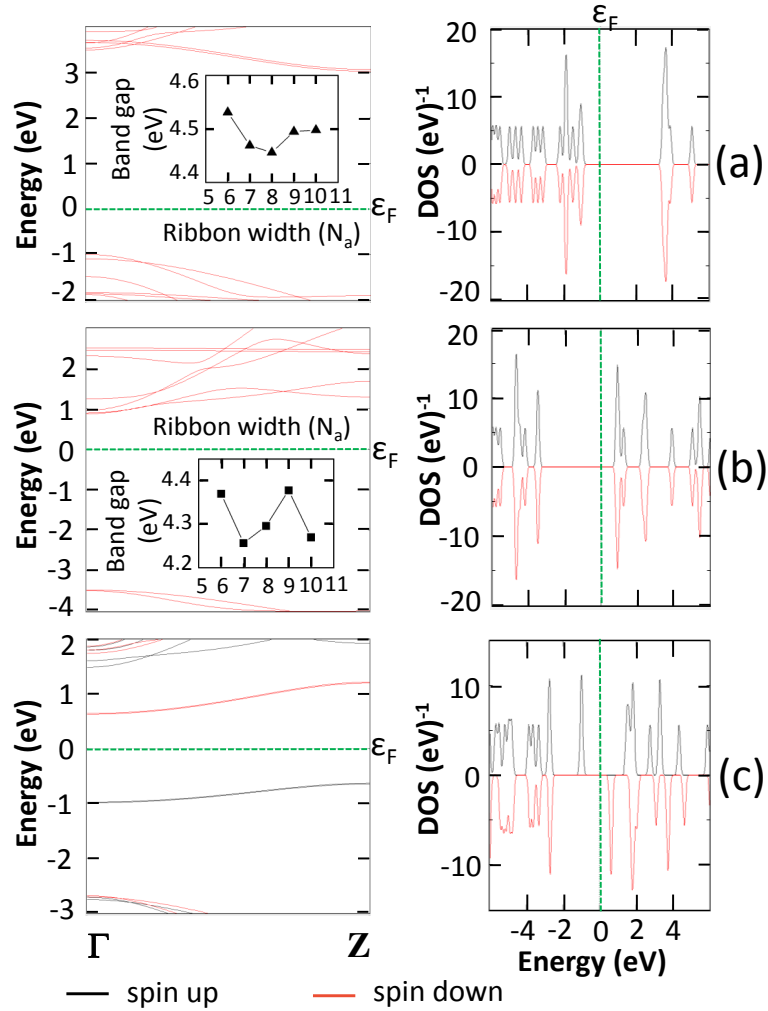


Figure 3. Calculated electronic band structures with corresponding density of states (DOS) for (a) bare 9-ABNNR, (b) 9- $ABNNR_{FBN}$, and (c) 9- $ABNNR_{FN}$. Inset; shows the width dependence of band gap for bare ABNNR and $ABNNR_{FBN}$. The Fermi level is indicated by green dotted line whereas spin-down (spin-up) states are shown with red (black) color.

the origin of half-metallicity in $ABNNR_{FB}$ structures, we analyzed how the passivation of edge atoms affects the band structure and DOS. The passivation of edge N atoms with F mainly shifts α band/state away from the Fermi level while the change in the position of β band/state depend also upon passivation of edge-B atoms (Figure 1 and 2). Projected DOS (PDOS) analysis reveals that both of these bands are predominantly

composed of $2p$ orbitals of un-passivated edge N atoms. Moreover, we have estimated the bare on site Coulomb repulsion [25,36] as a difference between the first order ionization energy and electron affinity [25,37] for each element individually. The estimated values are 14.01 eV for F, 8.02 eV for B and 14.79 eV for N. This large difference (≥ 5.99 eV) between N/F and B atoms inhibits the charge transfer through edge-B atoms/B-F bond; therefore, the electrons are localized only in $2p$ orbital of N atoms. This mechanism for origin of half-metallicity is consistent with PDOS analysis and previous reports [25,38] on BNNRs. For the further confirmation of charge localization in bare

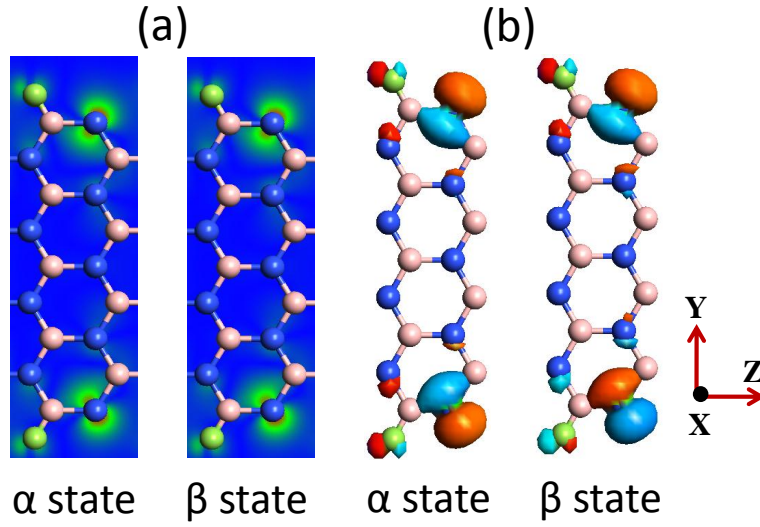


Figure 4. Calculated Bloch states for 9-ABNNR_{FB} presented in the form of (a) Contour and (b) Isosurface. The isovalue is 0.09 (au).

edge-N atoms Bloch states have been calculated as shown (for $N_a=9$) in Figure 4. The 9-ABNNR_{FB} supercell unit [Figure 1(c)] consists of 9 B, 9 N and 2 F atoms. A single B (N) atom contributes three (five) valence electrons as its electronic configuration is $2s^22p^1$ ($2s^22p^3$) whereas a single F atom seven valence electrons - $2s^22p^5$. Thus there are total 86 valence electrons in the system. Each band is doubly degenerate (considering spin) and hence there will be 43 valence bands in all. Therefore, the band index, which we used in calculations, for valence band maximum (VBM) is 42 (α band/state) and 43 (β band/state) for conduction band minimum (CBM) as indexing starts from zero. The presented Bloch states calculations are performed for k-points value of (0.0, 0.0, 0.5). The contour and isosurface, shown in Figure 4 (a) and (b) respectively, are more or less identical (charge localization) for α and β bands as both of these bands are correspond to the same spin states (downspin) across the Fermi level. It can be clearly seen from contour and isosurface that the unpaired electrons are mainly localized at the bare edge-N atoms. The interchanged colors of Bloch states for α and β states, at bottom ribbon edge, indicate separation of these states via Fermi level. Conversely, colors, at

the top ribbon edge, are same for α and β states which probably point towards the encroachment of α state into CB. A little charge localization is also appearing around F and near edge N atoms but it has no contribution across the Fermi level as confirmed via PDOS analysis. In addition, the distance between any two adjacent edge N atoms (~ 2.4 Å) is large enough to ensure that no edge reconstruction has taken place, and there is consequently only one dangling bond per edge-N atom is present. This analysis implies that the half-metallic spin polarization in ABNNR_{FB} structures is entirely attributed to the localization of unpaired electron at bare edge-N atoms.

We also assess the effect of different kinds of edge F-passivation on magnetic properties of bare ABNNRs. The magnetic moment M (μ_B) and energy difference ΔE (eV) between spin polarized (E_{LSDA}) and spin compensated states (E_{LDA}) for the most stable edge fluorinated ribbon configuration (ABNNR_{FB}) are presented in Table 2. A noteworthy net magnetic moment of about $2.03 \mu_B$ is witnessed for all ABNNR_{FB} structures on the contrary, ABNNR_{FBN} do not possess any magnetism. In addition, a net magnetic moment of about $2.02 \mu_B$ is also perceived in ABNNR_{FN} . It is worth noticing here that the latter magnetic moment probably have little practical significance as it is observed in ABNNR_{FN} structures which are 330 meV less stable as compare to ABNNR_{FB} structures. Present non-d orbital type of magnetism observed in ABNNR_{FB} structures is accounted for the magnetic moment of unpaired electrons localized in bare edge-N atoms. This is consistent with giant splitting of spin states [Figure 2(b) and 3(c)] and localization of electrons as discussed in Bloch state analysis. It is clear from Table 2 that the spin polarized state is ~ 0.4 eV ($\Delta E = |E_{LSDA} - E_{LDA}|$) more stable with respect to the spin un-polarized state (E_{LDA}). This ΔE is remarkably large in comparison to the values (0.17 eV, 48 meV and 3.5 meV) reported [24,27,29] for ZBNNRs, which qualifies present ABNNR_{FB} structures as better candidates for spintronics applications. Moreover, the coupling between electrons of inter-edge bare N atoms may be either ferromagnetic or antiferromagnetic, as the observed energies are very close to each other. In sum, we reveal that the electronic and magnetic properties of ABNNRs critically depend on the type of edge fluorination, as summarized in Table 3.

4. Conclusions

Conclusively, the effect of edge fluorination on the electronic and magnetic properties of ABNNRs has been investigated systematically using ab-initio calculations. ABNNR_{FB} are found half metallic and energetically most favorable, with a half metal gap of 0.3 eV. The spin polarized states are more stable by ~ 0.4 eV as compared to spin compensated states (E_{LDA}) which projects these half-metallic ribbons as promising building blocks for spin based electronic devices. Passivation of only edge-B (N) atoms with F atoms i.e. ABNNR_{FB} (ABNNR_{FN}) transforms insulating bare ABNNRs into half-metal (wide band gap semiconductor) and also causes the splitting of spin states which gives rise to a substantial net magnetic moment of about 2.03 (2.02) μ_B . Conversely, both-edge

F-passivation does not alter electronic or magnetic behavior significantly; therefore, $\text{ABNNR}_{\text{FBN}}$ structures are insulators with degenerate/symmetric spin states similar to bare ABNNRs. Owing to the promising potential of spin polarization, we expect experimental realization of half-metallicity in ABNNRs via edge fluorination.

Acknowledgements

Authors thank sophisticated instrumentation center (SIC), IIT Indore for SEM & PL measurements. One of the authors (GS) would like to acknowledge DST, Govt. of India, for the funding under DST Fast Track Scheme for Young Scientists, Project No. SR/FTP/PS-007/2012.

References

- [1] W. Auwarter, H. U. Suter, H. Sachdev, and T. Greber, *Chem. Mater.* 16, 343 (2003).
- [2] D. Pacil, J. C. Meyer, . . . Girit, and A. Zettl, *Appl. Phys. Lett.* 92, 133107 (2008).
- [3] W.-Q. Han, L. Wu, Y. Zhu, K. Watanabe, and T. Taniguchi, *Appl. Phys. Lett.* 93, 223103 (2008).
- [4] Y. Lin and J. W. Connell, *Nanoscale* 4, 6908 (2012).
- [5] Z.-G. Chen, J. Zou, G. Liu, F. Li, Y. Wang, L. Wang, X.-L. Yuan, T. Sekiguchi, H.-M. Cheng, and G. Q. Lu, *ACS Nano* 2, 2183 (2008).
- [6] M. Y. Han, B. zyilmaz, Y. Zhang, and P. Kim, *Phys. Rev. Lett.* 98, 206805 (2007).
- [7] N. K. Jaiswal and P. Srivastava, *IEEE Trans. Nanotechnol.* 12, 685 (2013).
- [8] N. K. Jaiswal and P. Srivastava, *Solid State Commun.* 152, 1489 (2012).
- [9] X. Wu, M. Wu, and X. C. Zeng, *Front. Phys. China* 4, 367 (2009).
- [10] H. M. Rai, N. K. Jaiswal, P. Srivastava, and R. Kurchania, *J. Comput. Theor. Nanosci.* 10, 368 (2013).
- [11] Z. Zhang, W. Guo, and B. I. Yakobson, *Nanoscale* 5, 6381 (2013).
- [12] X. Lin and J. Ni, *Phys. Rev. B* 84, 075461 (2011).
- [13] Y. Liu, X. Wu, Y. Zhao, X. C. Zeng, and J. Yang, *J. Phys. Chem. C* 115, 9442 (2011).
- [14] C. Len and A. Latg, *Phys. Rev. B* 88, 245446 (2013).
- [15] X. Li, X. Wu, and J. Yang, *J. Am. Chem. Soc.* 136, 5664 (2014).
- [16] R. A. de Groot, F. M. Mueller, P. G. van Engen, and K. H. J. Buschow, *Phys. Rev. Lett.* 50, 2024 (1983).
- [17] V. Alijani, J. Winterlik, G. H. Fecher, S. S. Naghavi, and C. Felser, *Phys. Rev. B* 83, 184428 (2011).
- [18] K.-I. Kobayashi, T. Kimura, H. Sawada, K. Terakura, and Y. Tokura, *Nature* 395, 677 (1998).
- [19] K.-I. Kobayashi, T. Kimura, Y. Tomioka, H. Sawada, K. Terakura, and Y. Tokura, *Phys. Rev. B* 59, 11159 (1999).
- [20] I. Galanakis and P. Mavropoulos, *Phys. Rev. B* 67, 104417 (2003).
- [21] W.-H. Xie, Y.-Q. Xu, B.-G. Liu, and D. G. Pettifor, *Phys. Rev. Lett.* 91, 037204 (2003).
- [22] B.-G. Liu, in *Half-Met. Alloys*, edited by I. Galanakis and P. D. P. H. Dederichs (Springer Berlin Heidelberg, 2005), pp. 267291.
- [23] M. Jourdan, J. Minr, J. Braun, A. Kronenberg, S. Chadov, B. Balke, A. Gloskovskii, M. Kolbe, H. J. Elmers, G. Schnhense, H. Ebert, C. Felser, and M. Klui, *Nat. Commun.* 5, (2014).
- [24] F. Zheng, G. Zhou, Z. Liu, J. Wu, W. Duan, B.-L. Gu, and S. B. Zhang, *Phys. Rev. B* 78, 205415 (2008).
- [25] Y. Wang, Y. Ding, and J. Ni, *Phys. Rev. B* 81, 193407 (2010).
- [26] V. Barone and J. E. Peralta, *Nano Lett.* 8, 2210 (2008).
- [27] W. Chen, Y. Li, G. Yu, C.-Z. Li, S. B. Zhang, Z. Zhou, and Z. Chen, *J. Am. Chem. Soc.* 132, 1699 (2010).
- [28] L. Lai and J. Lu, *Nanoscale* 3, 2583 (2011).
- [29] D. K. Samarakoon and X.-Q. Wang, *Appl. Phys. Lett.* 100, 103107 (2012).
- [30] Z. M. Liu, Y. Zhu, and Z. Q. Yang, *J. Chem. Phys.* 134, 074708 (2011).
- [31] Y. Ding, Y. Wang, and J. Ni, *Appl. Phys. Lett.* 94, 233107 (2009).
- [32] M. Brandbyge, J.-L. Mozos, P. Ordejn, J. Taylor, and K. Stokbro, *Phys. Rev. B* 65, 165401 (2002).
- [33] J. P. Perdew and A. Zunger, *Phys. Rev. B* 23, 5048 (1981).
- [34] J. Zhao, A. Buldum, J. Han, and J. P. Lu, *Nanotechnology* 13, 195 (2002).
- [35] Y.-W. Son, M. L. Cohen, and S. G. Louie, *Nature* 444, 347 (2006).
- [36] S. Dutta, A. K. Manna, and S. K. Pati, *Phys. Rev. Lett.* 102, 096601 (2009).
- [37] The data of ionization energy and electron affinity is adopted from http://chemed.chem.purdue.edu/genchem/topicreview/bp/ch7/ie_ea.html
- [38] F. Zheng, K. Sasaki, R. Saito, W. Duan, and B.-L. Gu, *J. Phys. Soc. Jpn.* 78, 074713 (2009).

Ribbon width N_a	E_c (eV)			
	Bare ABNNR	ABNNR _{FBN}	ABNNR _{FB}	ABNNR _{FN}
6	-9.52	-8.54	-9.08	-8.56
7	-9.62	-8.73	-9.22	-8.77
8	-9.70	-8.87	-9.33	-8.93
9	-9.75	-9.00	-9.41	-9.06
10	-9.80	-9.10	-9.49	-9.16

Table 1. Calculated cohesive energies (eV) as a function of ribbon width for all considered ribbon structures.

	$N_a = 6$	$N_a = 7$	$N_a = 8$	$N_a = 9$	$N_a = 10$
M(μ_B)	2.03	2.04	2.03	2.03	2.03
ΔE (eV)	0.41	0.38	0.40	0.42	0.41

Table 2. Calculated magnetic moment and energy difference ($\Delta E = |E_{LSDA} - E_{LDA}|$) between spin polarized and spin un-polarized states for most stable ABNNR_{FB} with different widths.

Ribbon Configuration	Avg. M(μ_B)	Electronic state	Band gap (eV)	magnetic state
Bare ABNNR	0	Insulator	4.46 – 4.53	Non-magnetic
ABNNR _{FBN}	0	Insulator	4.26 – 4.38	Non-magnetic
ABNNR _{FB}	2.03	Half-metal (0.3 eV)	0	Magnetic
ABNNR _{FN}	2.02	Wide bandgap semiconductor	3.16 – 3.34	Magnetic

Table 3. The overall magnetic and electronic behavior for all considered bare and fluorinated ABNNRs ($N_a = 6$ to 10).